

Commensurate to Incommensurate Charge Ordering and Its Real-Space Images in $\text{La}_{0.5}\text{Ca}_{0.5}\text{MnO}_3$

C. H. Chen and S-W. Cheong

Bell Laboratories, Lucent Technologies, Murray Hill, New Jersey 07974

(Received 24 January 1996)

The antiferromagnetic to ferromagnetic transition in $\text{La}_{0.5}\text{Ca}_{0.5}\text{MnO}_3$ is accompanied by a commensurate to incommensurate charge-ordering transition. The presence of incommensurate charge correlation in the ferromagnetic phase is a remarkable interplay between charge and spin in double-exchange ferromagnets. Furthermore, a dark-field imaging technique has provided real-space images of charge-ordered domains revealing discommensurations inside the nearly commensurate domains. Local density fluctuations of discommensurations are responsible for the similar variations of the charge-ordering wave vector. [S0031-9007(96)00232-3]

PACS numbers: 75.30.Kz, 64.70.Rh, 71.38.+i, 75.50.Cc

Charge carrier doping in antiferromagnetic (AFM) insulators, particularly through heterovalent ion substitution in transition metal oxides with perovskite-related structure, has revealed extraordinary phenomena such as high temperature superconductivity, electronic phase separation, and charge ordering. For example, hole carriers superconduct in layered $\text{La}_{1.85}\text{Sr}_{0.15}\text{CuO}_4$ at ~ 40 K [1], and holes undergo a charge-ordering transition in isostructural $\text{La}_{1.67}\text{Sr}_{0.33}\text{NiO}_4$ at ~ 240 K [2] with indications of electronic phase separation [3]. Another remarkable behavior of doped charge carriers was discovered recently in three-dimensional perovskite $\text{La}_{1-x}\text{Ca}_x\text{MnO}_3$ [4,5]. LaMnO_3 is an AFM insulator and carrier doping via Ca substitution in La sites with $0.2 < x < 0.5$ results in the occurrence of "colossal" magnetoresistance (CMR) [4]. $\text{La}_{1-x}\text{Ca}_x\text{MnO}_3$ is a paramagnetic insulator at high temperatures. At low temperatures, the material is a ferromagnetic (FM) metal in the doping range where CMR occurs, and for $x > 0.5$, the ground state is an AFM insulator [5,6]. A phase boundary between the FM metallic and the AFM insulating ground states exists in a narrow range around $x = 0.5$. In fact, the $x = 0.5$ compound first undergoes a FM transition upon cooling and then follows a first-order transition to an AFM charge-ordered state at ~ 135 K (~ 180 K on warming) [5,7].

In this paper, we report that the AFM to FM transition in $\text{La}_{0.5}\text{Ca}_{0.5}\text{MnO}_3$ is structurally associated with a commensurate to incommensurate charge-ordering phase transition. The presence of incommensurate charge ordering in the FM phase is a new finding that could shed light on the intriguing interplay among charge, spin, and lattice in the system. Furthermore, we have obtained real space images of the charge-ordered phase using the superlattice dark-field imaging technique. Configurations of charge-ordered domains (COD's) with the presence of discommensurations (DC's) were observed in the nearly commensurate phase. Local fluctuations of DC densities were commonly observed and found to be responsible for similar variations of the charge-ordering wave vector—a common occurrence in various charge-ordered systems.

Both ceramic and single-crystalline samples were used for the present study, and essentially the same results were obtained. The ceramic samples were synthesized by a solid state reaction. Single crystals were grown by a floating zone technique. Samples for electron diffraction and dark-field imaging were prepared by mechanical polishing followed by ion milling at liquid nitrogen temperature. A JEOL 2000 FX electron microscope equipped with a low temperature sample stage and a 14-bit charge coupled device array detector was used. The sample in the electron microscope is located inside an objective lens with a magnetic field of ~ 2 T.

The diffraction evidence of the charge ordering in $\text{La}_{0.5}\text{Ca}_{0.5}\text{MnO}_3$ is shown in Fig. 1(a) which represents a [001] zone-axis electron diffraction pattern obtained at 95 K. The diffraction pattern can be indexed with the known orthorhombic crystal structure [8] (space group $Pbnm$) of $\text{La}_{0.5}\text{Ca}_{0.5}\text{MnO}_3$ with $a \approx b \approx \sqrt{2} a_p$ and $c \approx 2a_p$ (where $a_p \sim 3.9$ Å is the lattice parameter of the simple perovskite structure). We made no attempts to distinguish the a and b lattice parameters due to the small orthorhombic distortion that cannot be readily resolved in a typical electron diffraction experiment. In Fig. 1(a), sharp superlattice spots are evident in addition to the fundamental Bragg reflections. Furthermore, the wave vector \vec{q} of the superlattice modulation was found to be nearly commensurate at this temperature and can be written as $\vec{q} = (2\pi/a)(1/2 - \epsilon, 0, 0)$ with incommensurability parameter $\epsilon = 0.013$. In the tetragonal cell notational, the superlattice peaks occur near $(\pi/2, \pi/2)$. Results obtained from selected-area electron diffraction experiments show that ϵ could vary slightly from grain to grain and area to area even within the grain. Commensurate charge ordering with $\epsilon = 0$ was often observed. We have also determined that the two perpendicular sets of superlattice spots around each fundamental Bragg reflection actually originate from different areas of the sample. We will elaborate on this point later when we discuss the real space results obtained from dark-field images. The detection of superlattice spots at low temperatures provides

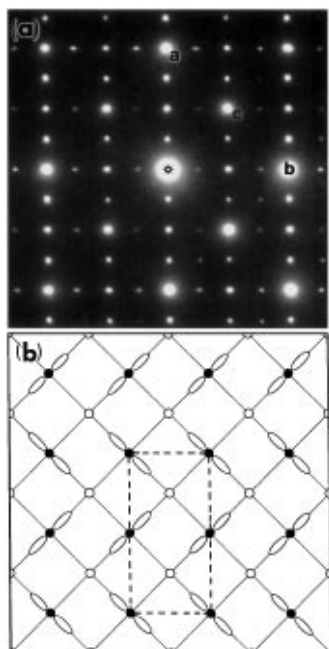


FIG. 1. (a) [001] zone-axis electron diffraction pattern obtained at 95 K. The fundamental Bragg peaks labeled a , b , and c can be indexed as (200) , (020) , and (110) , respectively. The presence of superlattice spots with modulation wave vector $(1/2, 0, 0)$ or $(0, 1/2, 0)$ is evident. Kinematically forbidden (100) and (010) spots also appear as a result of multiple scattering. (b) Schematic charge-ordering picture of Mn^{4+} and Mn^{3+} ions. Open and closed circles represent Mn^{4+} and Mn^{3+} ions, respectively. The orientational order of d_{z^2} orbitals of Mn^{3+} ions which results in the cell doubling along the a axis is also indicated.

direct structural evidence of charge ordering as suggested from previous indirect transport and magnetic susceptibility measurements [5]. In $\text{La}_{0.5}\text{Ca}_{0.5}\text{MnO}_3$, there are just as many Mn^{4+} ($3d^3$) ions as Mn^{3+} ($3d^4$) ions. We show in Fig. 1(b) a schematic picture of ionic ordering of Mn^{4+} and Mn^{3+} consistent with the ordering wave vector of $\vec{q} = (2\pi/a)(1/2, 0, 0)$. Previously, it was proposed that the cell doubling along the a axis could be achieved by the orientational ordering of d_{z^2} orbitals in Mn^{3+} , in addition to the Mn^{4+} - Mn^{3+} ionic ordering [9,10].

The first-order FM-AFM transition is characterized by a substantial thermal hysteresis in the temperature-dependent resistivity and magnetization measurements [5]. To establish the correlation between the presence of charge-ordering superlattice peaks and the FM-AFM transition, we have followed the superlattice peaks and measured the charge-ordering wave vector as a function of temperature during cooling and warming. The results are shown in Fig. 2 in which the incommensurability of charge ordering, ε , is plotted as a function of temperature. Figure 2 clearly shows that the first-order FM-AFM transition is associated structurally to an incommensurate-commensurate charge-ordering transition. Upon cooling from room temperature, precursory incommensurate charge-ordering superlattice peaks first become visible below ~ 240 K, with ε decreasing rapidly toward the

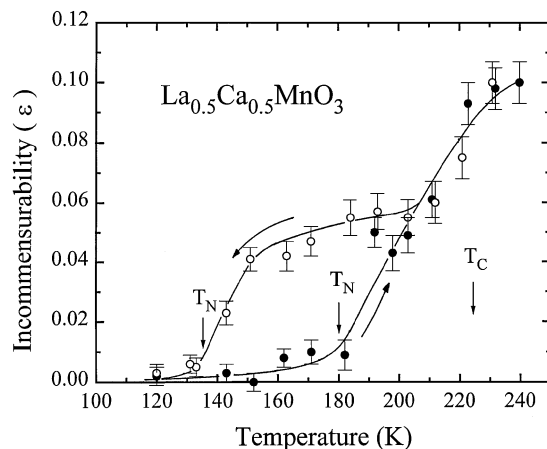


FIG. 2. Superlattice wave-vector incommensurability as a function of temperature upon cooling (open circles) and warming (closed circles). Lines are drawn as guides to the eye. The Curie temperature T_C and Néel temperatures T_N upon cooling and warming, determined from magnetic susceptibility measurement in 2 T, are also indicated.

FM transition at 220 K below which ε decreases rather slowly until 150 K. Below 150 K, ε decreases rapidly, and a commensurate charge-ordered state ($\varepsilon = 0$) is observed below 130 K. Due to spatial fluctuations of the charge-ordering wave vector, the charge-ordered state at lower temperatures is not always commensurate, and nearly commensurate states are often observed. In that case, the incommensurate-commensurate transition described above will become an incommensurate-nearly commensurate transition. Upon warming, ε remains commensurate ($\varepsilon = 0$) until $T \sim 180$ K, above which the charge ordering becomes incommensurate, and ε increases rapidly and coincides with the cooling curve above 210 K within the experimental uncertainties. The commensurate-incommensurate charge-ordering temperatures at 130 and 180 K upon cooling and warming, respectively, correlate well with FM-AFM transition temperatures determined by magnetization and resistivity measurements [5]. Intensity measurements of superlattice peaks during cooling and warming also reveal similar hysteresis with weaker intensities in the FM regime. In a recent x-ray and neutron powder diffraction experiment on $\text{La}_{0.5}\text{Ca}_{0.5}\text{MnO}_3$ [11], anomalous broadening of fundamental Bragg peaks was observed at the FM-AFM transition. We believe that the broadening is also related to the commensurate-incommensurate charge-ordering transition.

We emphasize that the temperature dependence of ε shown in Fig. 2 is not due to chemical inhomogeneity of Ca doping. Ca inhomogeneity, if it exists, cannot vary below room temperature because of the low mobility of Ca cations at low temperatures. Furthermore, electron beam microanalysis with a ~ 300 Å probe did not detect any chemical inhomogeneity of La and Ca ions in this area. A similar temperature dependence of incommensurability with similar magnitude has also been observed in the

nonmagnetic ferroelectric insulator of barium sodium niobate [12]. First-principles theoretical studies [13] indicated that the incommensurate behavior in insulators was caused by the relaxation of highly unstable structural units exhibiting angstrom-size displacements with essentially zero energy change. Similar mechanisms may also be responsible for the incommensurate behavior observed in our case.

The appearance of commensurate charge modulation with the high intensity of superlattice reflections in the AFM insulating phase is a familiar scenario since the report of charge ordering in the two-dimensional nickelates [2]. Charge-ordering phenomenon, however, is mutually exclusive with ferromagnetism, particularly in the double exchange process [14] which requires transfer of a charge carrier (hole) from a Mn^{3+} ion across an intervening O^{2-} ion to an adjacent Mn^{4+} ion. The FM coupling induced by itinerant charge carriers in the double-exchange scenario is totally incompatible with the localized picture of a commensurate charge-ordering state. We have carried out electron diffraction experiments for the $x = 0.33$ sample with an FM ground state and we found no superlattice reflections due to charge ordering at low temperatures. In the present case of $x = 0.5$, it is surprising that incommensurate charge ordering superlattice spots are present in the FM region. The energies involved for the FM ordering and incommensurate charge ordering may be degenerate around 225 K. As the temperature decreases, the incommensurate charge correlation gradually becomes more prominent with decreasing incommensurability and, at ~ 135 K, it becomes commensurate with the disappearance of ferromagnetism.

Let us now turn to dark-field imaging of the COD's and the DC's in the nearly commensurate phase. Figures 3(a) and 3(b) show dark-field images obtained at 95 K in the nearly commensurate phase from superlattice spots perpendicular to each other. The large brighter domains are areas that diffract strongly to the chosen superlattice spot. The most striking feature of the dark-field images is the presence of large rectangular COD's of a few thousand angstroms in size. The complementary domain contrast shown in Figs. 3(a) and 3(b) is direct proof that the two perpendicular sets of superlattice spots actually come from twin-related regions of the sample. The boundaries of the COD's are found to be more or less parallel to the Mn-O-Mn direction of the simple perovskite structure, which is 45° off the charge-ordering wave vector. This orientation becomes the natural choice of COD boundaries in view of the twinning structure of the COD's. The presence of impurities, defects, and local strains, however, can alter the orientation of the straight domain boundaries into other directions. The curved boundaries visible in Figs. 3(a) and 3(b) are probably the results of these extrinsic effects. It is important to note that the COD structure can only be observed from the superlattice reflections (not from the main Bragg peaks) and, therefore, they are directly associated with the charge ordering of doped holes.

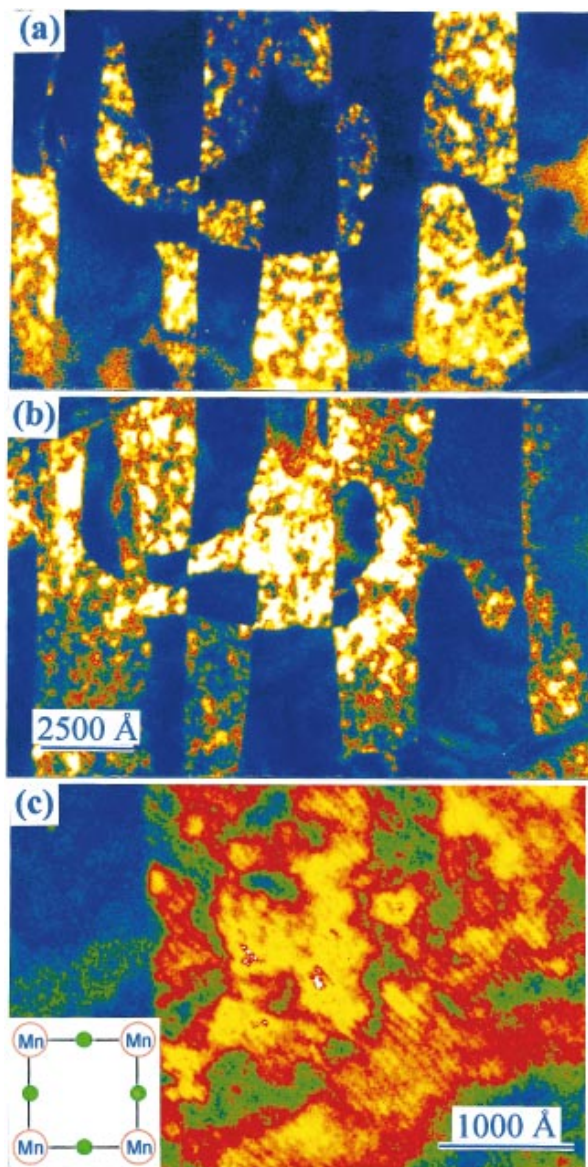


FIG. 3 (color). (a),(b) Color-coded complementary dark-field images obtained from superlattice peaks that are perpendicular to each other. (c) The quasiperiodic discommensurations in the charge-ordered domains. The visibility of discommensurations is sensitive to the variations of local diffraction conditions. The crystallographic orientation of the discommensurations and the charge-ordered domains relative to the Mn-O square lattice is also shown.

The domain boundaries shown in Figs. 3(a) and 3(b) are not to be confused with domain walls or DC's often seen in an incommensurate or nearly commensurate modulation. In a discommensurate state of an incommensurate modulation, small commensurate domains are separated by discommensurations within which the modulation superlattice phase varies rapidly [15]. The existence of DC's in the charge-ordered perovskite transition metal oxides is still a matter of conjecture. In Fig. 3(c), we show unequivocally the presence of DC's in the nearly commensurate state of charge ordering. The dark-field image of Fig. 3(c) was obtained under

similar conditions of 3(a) and 3(b). However, it was taken at a higher magnification to resolve the fine spacing of DC's. The dark stripes which separate the white stripes are identified as DC's, where the modulation superlattice phase varies rapidly, and the white stripes are commensurate regions where the modulation phase factor remains constant. DC's have also been directly observed in charge-density-wave systems [16,17] by the same superlattice dark-field imaging technique. The DC's, being perpendicular to the charge-ordering wave vector, are oriented in a direction 45° from the domain boundaries, i.e., along the diagonal of the Mn-O square lattice. The average spacing of DC's is $\sim 80 \text{ \AA}$ as measured from Fig. 3. For a discommensurate system, the average system, the average spacing, L , of DC's is related to the incommensurability ε (in the units of $2\pi/a$) through the relationship $L = 2\pi/p\varepsilon$ [15], where p is the order of commensurability and, in the present case, $p = 2$. For the single-crystalline sample used in our study, ε is found to be 0.034, and this gives rise to a $L \approx 80 \text{ \AA}$, in excellent agreement with the value observed in the dark-field image. The DC's shown in Fig. 3(c) actually extend throughout the thickness of the sample, and the images are, therefore, two-dimensional projections of these structures. Similar dark-field imaging of the incommensurate phase in the FM temperature region is much more difficult due to weak superlattice spots. We have, however, managed to obtain images in the FM regime showing the presence of DC's which become weaker, denser, and more disordered as temperature increases. We note that DC's in the charge-ordered state appear to be strongly pinned to the lattice without any noticeable movement even under intense electron beam irradiation during the dark-field observations, unlike the DC's in the charge-density-wave systems where their movement could be seen under similar conditions [16,17]. Samples examined with $0.5 < x \leq 0.67$ also show an incommensurate charge-ordered state, and presence of discommensuration is a universal phenomenon.

The charge-ordering incommensurability ε is found to vary from area to area. This has been an outstanding unsolved problem since the report of charge ordering in the two-dimensional $\text{La}_{2-x}\text{Sr}_x\text{NiO}_4$ [2]. Now, with the real-space imaging technique, we have discovered that this phenomenon occurs as a result of slight local density fluctuations of DC's. Even in a commensurate region where $\varepsilon = 0$, as determined from selected area electron diffraction, widely separated residual DC's are still present. The underlying reasons for the local density fluctuations of DC's remains unclear. We note, however, the length scale of the fluctuations is typically a few thousand angstroms, and preliminary electron beam microanalysis does not reveal any significant chemical inhomogeneity of this length scale. Furthermore, no obvious crystalline defects are present in the sample that can be responsible for the fluctuations. In charge-density-wave systems, similar DC density fluctuations do not occur [16,17].

In conclusion, much remains to be understood for the nearly commensurate to incommensurate charge-ordering transition in $\text{La}_{0.5}\text{Ca}_{0.5}\text{MnO}_3$, which coincides with the AFM to FM transition. The unexpected coexistence of incommensurate charge correlation and ferromagnetism provides an intriguing new phenomenon of charge-spin fluctuations. Real-space images of COD's with the presence of DC's reveals the discommensurate nature of the nearly commensurate charge-ordered state. Detailed configurations of DC's in the charge-ordered state, i.e., how DC's join to each other, might be interesting since it could be different from that observed in the conventional charge-density-wave system [16,17] due to the discrete lattice sites available for the ordered charge carriers.

We thank W. Bao for sample preparation and L. W. Rupp, Jr., for susceptibility measurement. We have benefited from discussions with T. M. Rice, B. Batlogg, A. P. Ramirez, and P. E. Schiffer.

-
- [1] J. G. Bednorz and K. A. Müller, *Z. Phys. B* **64**, 189 (1986).
 - [2] C. H. Chen, S-W. Cheong, and A. S. Cooper, *Phys. Rev. Lett.* **71**, 2461 (1993); S-W. Cheong, H. Y. Hwang, C. H. Chen, B. Batlogg, L. W. Rupp, Jr., and S. A. Carter, *Phys. Rev. B* **49**, 7088 (1994).
 - [3] V. J. Emery, S. A. Kivelson, and H. Q. Lin, *Phys. Rev. Lett.* **64**, 475 (1990).
 - [4] S. Jin *et al.*, *Science* **264**, 413 (1994); R. von Helmolt *et al.*, *Phys. Rev. Lett.* **71**, 2831 (1993); K. Chahara *et al.*, *Appl. Phys. Lett.* **63**, 1990 (1993); R. M. Kusters *et al.*, *Physica (Amsterdam)* **155B**, 362 (1989).
 - [5] P. E. Schiffer, A. P. Ramirez, W. Bao, and S-W. Cheong, *Phys. Rev. Lett.* **75**, 3336 (1995).
 - [6] E. O. Wollan and W. C. Koehler, *Phys. Rev.* **100**, 545 (1955).
 - [7] A. P. Ramirez, P. Schiffer, S-W. Cheong, C. H. Chen, W. Bao, T. T. M. Palstra, B. Zegarski, P. L. Gammel, and D. J. Bishop, *Phys. Rev. Lett.* **76**, 3188 (1996).
 - [8] G. Matsumoto, *J. Phys. Soc. Jpn.* **29**, 615 (1970).
 - [9] J. B. Goodenough, *Phys. Rev.* **100**, 564 (1955).
 - [10] E. Pollert, S. Krupicka, and E. Kuzmicova, *J. Phys. Chem. Solids* **43**, 1137 (1982).
 - [11] P. G. Radaelli, D. E. Cox, M. Marezio, S-W. Cheong, P. E. Schiffer, and A. P. Ramirez, *Phys. Rev. Lett.* **75**, 4488 (1995).
 - [12] J. Schneck, J. C. Toledano, C. Joffrin, J. Aubree, B. Joukoff, and A. Gabelotaud, *Phys. Rev. B* **25**, 1766 (1982).
 - [13] V. Katkanant, P. J. Edwardson, J. R. Hardy, and L. L. Boyer, *Phys. Rev. Lett.* **57**, 2033 (1986).
 - [14] C. Zener, *Phys. Rev.* **82**, 403 (1951).
 - [15] W. L. McMillan, *Phys. Rev. B* **14**, 1496 (1976).
 - [16] C. H. Chen, J. M. Gibson, and R. M. Fleming, *Phys. Rev. Lett.* **47**, 723 (1981); *Phys. Rev. B* **26**, 184 (1982).
 - [17] K. K. Fung, S. McKernan, J. W. Steeds, and J. A. Wilson, *J. Phys. C* **14**, 5417 (1981).